



Article

Milling of an Aluminium Matrix Composite Using MCD-Tipped Tools with Adjusted Corner and Minor Cutting Edge Geometries

Benjamin Clauß * and Andreas Schubert

Professorship of Micromanufacturing Technology, Department of Mechanical Engineering, Chemnitz University Technology, Reichenhainer Str. 70, 09126 Chemnitz, Germany; andreas.schubert@mb.tu-chemnitz.de

* Correspondence: benjamin.clauss@mb.tu-chemnitz.de; Tel.: +49-371-531-33173

Abstract: Aluminium matrix composites (AMCs) represent suitable materials for lightweight design applications. The abrasive ceramic reinforcements typically require diamond cutting materials to prevent excessive tool wear. In milling with diamond cutting materials the influence of cutting parameters was already examined to a significant extent. Investigations concerning the effect of modified tool geometries are limited and the potentials with regard to the geometrical and physical surface properties are unclear. Accordingly, experimental investigations in milling of a 10 vol.% SiC particle-reinforced aluminium wrought alloy EN AW-2017 T4 were addressed. The effect of modified corner and minor cutting edge geometries were investigated based on mono crystalline diamond (MCD)-tipped tools to benefit stable process conditions. The results indicated achievable areal roughness values in the range around 0.2 µm. Especially the application of the lowest cutting edge angle and a trailing minor cutting edge led to strong fluctuations of the surface parameters. The lowest valley void volumes were achieved with an arched minor cutting edge. Generally, finish machining led to stronger compressive residual stresses compared to the state prior to machining. The strongest increase was achieved using a corner radius combined with a straight minor cutting edge. It is concluded that reduced effective radii generating the surface enable an acceptable surface structure and strong compressive residual stresses and should be addressed in further investigations.

Keywords: aluminium matrix composite; mono crystalline diamond; particle-reinforced; silicon carbide; wrought alloy; powder metallurgical



Citation: Clauß, B.; Schubert, A. Milling of an Aluminium Matrix Composite Using MCD-Tipped Tools with Adjusted Corner and Minor Cutting Edge Geometries. *J. Compos. Sci.* **2021**, *5*, 235. <https://doi.org/10.3390/jcs5090235>

Academic Editors: Oscar Marcelo Suárez and Hongseok Choi

Received: 28 July 2021

Accepted: 30 August 2021

Published: 4 September 2021

Publisher's Note: MDPI stays neutral with regard to jurisdictional claims in published maps and institutional affiliations.



Copyright: © 2021 by the authors. Licensee MDPI, Basel, Switzerland. This article is an open access article distributed under the terms and conditions of the Creative Commons Attribution (CC BY) license (<https://creativecommons.org/licenses/by/4.0/>).

1. Introduction

1.1. Technical Impact, Economical Relevance, and Sustainability of AMCs

Aluminium matrix composites (AMCs) represent high-strength lightweight materials that enable design strategies to reduce moving loads, thus increasing efficiency in technical systems.

Singh, Chaitanya, and Kumar explained the high relevance of these materials with an increased specific strength and an improved high-temperature behaviour. In this context, particle-reinforced composites would be researched more intensively due to a higher isotropy of material properties compared to fibre-reinforced AMCs [1]. Akhil projected an increase in metal matrix composite (MMC)-applications of about 20% by 2020 for the reason of advances in machining and processing [2].

Schmidt et al. concluded that a significant market potential was given for powder metallurgically produced AMCs with regard to aerospace applications. The combined market potential of the leading aircraft manufacturers was estimated with about USD 160 billion, presuming suitable machining solutions as key to transfer [3].

Eventually, investigations on the sustainability of AMCs gain in relevance. Shishkin et al. investigated the recycling of fibre-reinforced AMCs. In this regard, waste

composites were ground to fragments as an initial recycling stage [4]. Guo, Liu, and Shu investigated the material properties of a particle-reinforced AMC subsequent to remelting. Similar material properties compared to the initial state indicated applicability as a recycling process [5].

1.2. Applicable Cutting Materials for Finishing of AMCs

Hung et al. and Yanming and Zehua investigated the turning of SiC particle-reinforced AMCs with a spectrum of cutting materials comprising high speed steels (HSS), cemented carbides, cubic boron nitride (CBN), and poly crystalline diamond (PCD). The investigations concluded that cutting materials with a higher hardness compared to the reinforcing particles are required, especially with higher average particle sizes [6,7].

Ding et al. and Bushlya et al. investigated the applicability of different CBN and PCD grades for turning of 20 vol.% SiC particle-reinforced AMCs. Both investigations concluded a higher wear resistance of PCD- compared to CBN-tipped tools and a reduced tendency to built-up edge formation [8,9].

Wang et al. investigated the performance of PCD grades with diamond particle sizes of 1 μm , 10 μm , and 25 μm for the machining of a 65 vol.% SiC particle-reinforced AMC. The results indicated that the PCD grade with medium sized particles performed superior in the investigated range [10].

Collins and Cook and Cooper et al. addressed the machining of different SiC particle-reinforced AMCs with PCD, mono and poly crystalline chemical vapour deposited diamond (CVD-D), mono crystalline diamond (MCD), and natural diamond (ND). Based on the results, mono crystalline cutting materials outperformed the poly crystalline alternatives. Under certain process conditions mono crystalline CVD-D achieved a significantly longer tool life compared to ND [11,12].

1.3. Turning and Milling of AMCs with Diamond Cutting Materials

Bushan focused on the cutting parameter influence in turning of an aluminium alloy EN AW-7075 reinforced with 10 wt.% SiC particles. Although an increased cutting speed resulted in reduced R_a -values, higher feed values entailed an increased surface roughness [13].

Ge et al. examined milling of a SiC particle-reinforced AMC with PCD-tipped tools. In the investigated range of cutting parameters with comparably high values for feed and depth of cut the affected surface layer provided a thickness of about 35 μm [14].

Wang et al. and Dong et al. investigated the milling of highly SiC particle-reinforced AMCs by milling with PCD-tipped tools. Wang et al. referred to reduced roughness values R_a with a higher cutting speed, but higher values with increased feed. The residual stress state in the generated surface was characterised by compressive residual stresses. Dong et al. indicated a stronger formation of imperfections with both increased cutting speed and feed due to pulled-out particles and near-surface voids [15,16].

Schubert et al. and Schubert and Nestler addressed turning of a SiC particle-reinforced AMC in T4 heat treatment condition with CVD-D-tipped tools. The composite consisted of an aluminium wrought alloy of the type EN AW-2124 reinforced with 25 vol.% ceramic particles. The examinations focused on the influence of the corner geometry, chip breaker geometries, and the feed. Accordingly, tool breaker and wiper geometries enabled lower surface roughness values with the formation of surface imperfections remaining unaffected. Especially small corner radii benefited reduced surface imperfections and the generation of stronger compressive residual stresses [17,18].

Clauß, Nestler, and Schubert examined the milling of an AMC with CVD-D-tipped tools. The matrix was provided by a powder metallurgically produced aluminium alloy EN AW-2017 reinforced with 10 vol.% SiC particles. Increased cutting speeds benefited the reduction in void formation on the generated surfaces. In the investigated range medium cutting speeds and feeds per tooth resulted in the strongest compressive residual stresses [19].

Ge et al. compared the application of PCD- and MCD-tipped tools for ultra precision turning of an aluminium cast alloy (EN AC-42100) and wrought alloy (EN AW-2024) reinforced with different proportions of SiC particles. The affected surface layer increased when using PCD as cutting material compared to MCD. However, subsequent to machining the micro hardness values in the surface layer were higher with regard to MCD [20].

Bian et al. applied MCD-tipped tools for ultra precision milling of a particle-reinforced AMC with 65 vol.% SiC particles with the feed per tooth and the depth of cut selected in the micrometer range. Although roughness values Ra in the nanometre range were achieved, surface imperfections occurred on the generated surface. Nonetheless, some of the cut particles indicated ductile mode separation [21].

Clauß et al. investigated the turn milling of a T4 heat treated 25 vol.% SiC particle-reinforced aluminium wrought alloy EN AW-2124 respecting different cutting parameters and clearance angles of the minor cutting edge. An increase in the cutting speed and a small axial feed led to a reduced formation of voids on the generated surface supported by a small clearance angle. Moreover, the combination of a small clearance angle and a small axial feed allowed for stronger compressive residual stresses. The results of EBSD analyses indicated grain refinement in the surface layer of the generated surface, fostered by higher cutting speeds [22].

Additionally, Clauß et al. focused on milling of a powder metallurgically produced AMC with MCD-tipped tools. The composite material consisted of an aluminium wrought alloy EN AW-2017 T4 and 10 vol.% SiC particles. The investigation examined the effect of different clearance and rake angles of the minor cutting edge in milling and the resulting influences of different material compositions. In this regard, milling with a positive rake angle and a higher particle proportion benefited stronger compressive residual stresses [23,24].

1.4. Inferences

The finishing of AMCs with acceptable efficiency and process stability requires the application of diamond cutting materials. Although there is a reasonable amount of research on the application of PCD, the number of investigations on binderless mono and poly crystalline cutting materials such as CVD-D and MCD is significantly lower. Moreover, there is a strong demand for an intensified examination on the influence of the tool geometry on the resulting surface properties, while there is already a considerable knowledge on the effect of the cutting parameters. Referring to that, the selection of MCD is highly suitable for cutting experiments. MCD provides the highest wear resistance against abrasion, thus enabling stable process conditions when investigating different tool geometries. The current research seeks to complement previous investigations in milling on the influence of clearance and rake angle of the minor cutting edge according to [23]. Complementary to that, the current investigations are focused on the geometry of the minor cutting edge and the cutting corner.

2. Materials and Methods

2.1. Composite Material Characterisation

The investigated specimen material is represented by a particle-reinforced aluminium matrix composite. The composite matrix is based on an aluminium wrought alloy comparable to the type EN AW-2017 with a composition of AlCu3.9Mg0.7Mn0.6. The reinforcement is realised using a commercially available and fully characterised fraction of SiC particles with an averaged size of $d_{90} < 2 \mu\text{m}$ (ESK-SiC GmbH, Frechen, Germany). In this regard, 90% of the contained particles provide a diameter less than $2 \mu\text{m}$. Additionally, Siebeck characterised the used particle fraction in his scientific work identifying a splintery character of the particle geometry ([25], p. 45). Referring to the composition of the AMC the proportion of the matrix and the reinforcements amounts 90 vol.% and 10 vol.%.

Hockauf et al. and Siebeck extensively researched the fabrication process during the Collaborative Research Centre SFB 692 HALS. For the production of the composite a powder metallurgical route was used mixing single components in powder state. In order

to achieve a homogeneous micro structure of the composite, first of all the components were subjected to high-energy ball milling. In this regard, a Simoloyer CM08 mill (ZoZ GmbH, Freudenberg, Germany) was used to realise a milling process at alternating rotational speeds of 400 min^{-1} and 700 min^{-1} at room temperature. In order to prevent contamination, both a ceramic ZrO_2 rotor and 5 mm ZrO_2 balls were used. The ball to powder ratio was given with 10/1 using stearic acid as separation agent. Subsequent to high energy milling the powder mixture was subjected to devolatilisation at $510 \text{ }^\circ\text{C}$ and a pressure of $6 \cdot 10^{-3} \text{ MPa}$ for 4 h. In a next step, the material was compacted by hot isostatic pressing applying a temperature of $450 \text{ }^\circ\text{C}$ and a pressure of 110 MPa for a time of 3 h. Furthermore, the compacted material was extruded with a ratio of 42.2:1 in order to achieve an improvement of the mechanical properties. Eventually, the AMC underwent heat treatment according to T4 procedure comprising solution annealing, quenching, and cold ageing [26], ([25], p. 35).

In Table 1, averaged values were summarised for the relevant mechanical parameters of the unreinforced matrix alloy and the particle-reinforced composite material.

Table 1. Mechanical properties of the investigated composite consisting of 90 vol.% EN AW-2017 + 10 vol.% SiC_p adapted from [23,24] and the assigned unreinforced matrix alloy.

Mechanical Parameters	EN AW-2017 T4	90 vol.% EN AW-2017 T4 + 10 vol.% SiC_p
Yield strength $R_{p0.2}$	348 MPa	467 MPa
Ultimate tensile strength R_m	502 MPa	610 MPa
Young's modulus E	71 GPa	90 GPa
Fracture elongation A_g	14.3%	8.6%
Vickers hardness HV	141 HV 10	182 HV 10
Initial first principal residual stress σ_{RS,I_0}	−67 MPa	−71 MPa
Initial second principal residual stress σ_{RS,II_0}	−20 MPa	−40 MPa

The presented values of the composite were determined based on ten measurements distributed over the material batch. The characterisation of the unreinforced matrix was based on three measurements. The loads during tensile testing were applied in the direction of extrusion. In difference to that, the hardness values and the initial residual stress states were measured perpendicular to the extrusion direction. In order to determine the initial residual stress state in the material, mechanically unaffected surfaces were generated by electro chemical machining (ECM). Figure 1 presents cross sections of the investigated composite material.

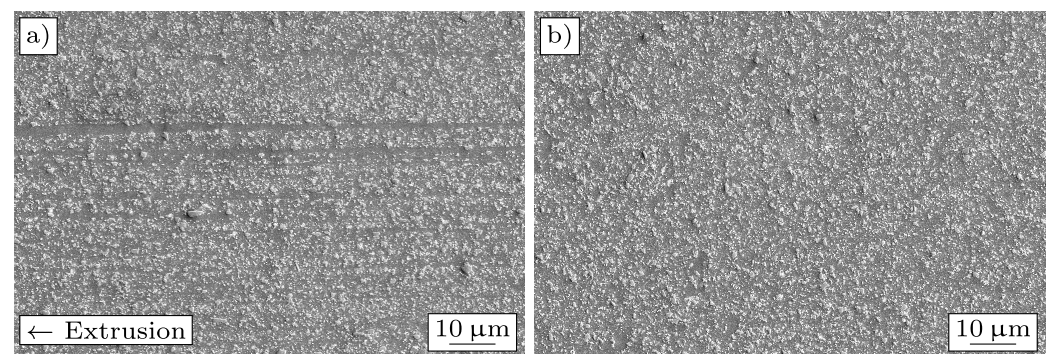


Figure 1. Microstructure of the investigated composite which was also addressed in previous investigations [23,24]. The figure presents scanning electron microscopy (SEM) images of cross sections (a) parallel and (b) perpendicular to the extrusion direction.

The microstructure exhibits homogeneously distributed ceramic particles with a particle size variation according to the given diameter range d_{90} . The extrusion process led

to the occurrence of banding effects in the microstructure parallel to the extrusion direction and thus increased anisotropy of the mechanical properties. Consequently, the generated surfaces in the cutting tests were oriented perpendicular to the extrusion direction to limit the influence of these effects.

2.2. Cutting Material and Tool Geometry

For the experimental investigations MCD is selected as cutting material, as the wear resistance is higher compared to PCD and CVD-D. Accordingly, the cutting material benefits a higher process stability, reproducibility, and decreasing unintended secondary effects due to overly extensive tool wear. For the experimental investigations single-edged tools (Medidia GmbH, Idar-Oberstein, Germany) with a nominal diameter of 3 mm were applied. The clearance angle, wedge angle, and rake angle of the minor cutting edge generating the specimen surface are kept unchanged with $\alpha'_o = 2^\circ$, $\beta'_o = 88^\circ$, and $\gamma'_o = 0^\circ$. The influence of adjusted cutting edge angles of the minor cutting edge on the resulting surface properties was investigated for values of $\kappa'_r = 1^\circ, 2^\circ$, and 3° . The influence of the cutting corner was examined based on a chamfer $F0.1 \text{ mm} \times 45^\circ$ and a corner radius R0.05. Eventually, the influence of different wiper geometries represented by a trailing minor cutting edge combined with a corner radius R0.05- $0^\circ \times 0.05$ and a combination of an arched minor cutting edge combined with a corner radius R0.05-R50 were taken into account. In order to enable a better understanding of the different geometries of the cutting corner and the minor cutting edge addressed in the current investigations Figure 2 presents the different tool variants.

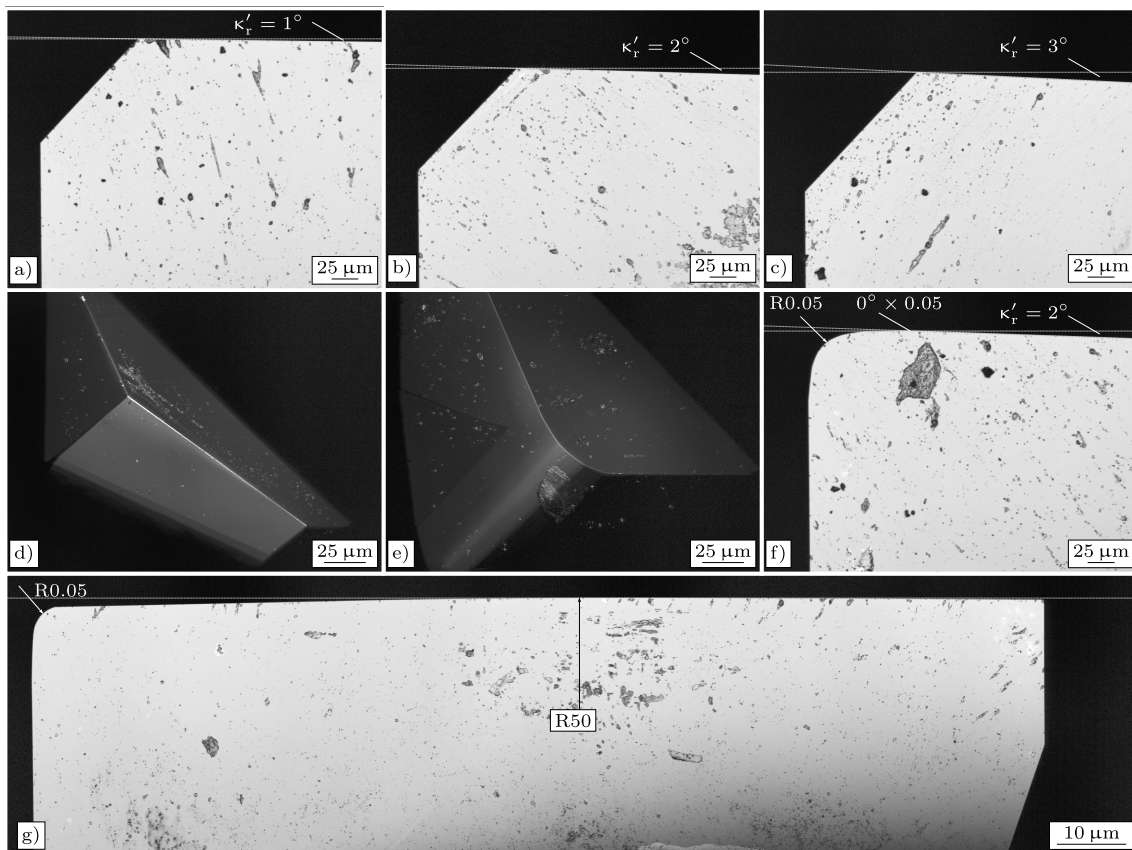


Figure 2. Different geometries of mono crystalline diamond (MCD)-tipped tools (a–c) chamfered corner and straight minor cutting edge with cutting edge angles $\kappa'_r = 1^\circ, 2^\circ$, and 3° , (d) corner chamfer $F0.1 \times 45^\circ$, (e) corner radius R0.05, (f) trailing cutting edge with corner radius R0.05- $0^\circ \times 0.05$, and (g) arched cutting edge with corner radius R0.05-R50.

2.3. Cutting Conditions and Experimental Setup

The milling tests were realised using a high precision milling centre of the type KERN Pyramid Nano (KERN Microtechnik GmbH, Eschenlohe, Germany). For all experimental investigations flood cooling was applied as cooling strategy based on an emulsion generated from Cimstar 501 concentrate (Cimcool Industrial Products B.V., Vlaardingen, The Netherlands). The specimen geometry is represented by cylindrical sections as illustrated according to Figure 3.

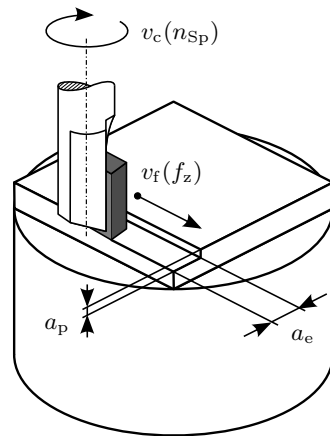


Figure 3. Applied specimen geometry and process kinematics for experimental investigations according to [23].

As a first step in each experiment, a CVD-D-tipped auxiliary tool (Diamond Tooling System GmbH, Kaiserslautern, Germany) was used to create the square specimen surface with an area of $(9 \times 9) \text{ mm}^2$. Subsequently, the MCD-tipped tools (Medidia GmbH, Idar-Oberstein, Germany) were used to machine each specimen with the predefined cutting parameters and the respective tool geometries. The investigated combinations of cutting parameters and tool geometries were summarised according to Table 2.

Table 2. Cutting parameters and tool geometries investigated in the experimental investigations.

v_c (m/min)	f_z (mm)	a_p (mm)	a_e (mm)	α'_0	γ'_0	κ'_r	Corner Geometry
250	0.015	0.25	0.5	2°	0°	1°	F0.1 × 45°
						2°	F0.1 × 45°
						3°	F0.1 × 45°
						2°	R0.05
						2/0°	R0.05-0° × 0.05
						-	R0.05-R50

2.4. Surface Evaluation

The surface structure of the generated surfaces was evaluated based on confocal laser scanning microscopy. For the acquisition of the primary surfaces an instrument of the type Keyence VK-9700 (Keyence Corporation, Osaka, Japan) was used. Subsequently, the surface data were processed and filtered using the surface evaluation software MountainsMap® (Digital Surf, Besançon, France). Referring to DIN EN ISO 25178-3 and based on the boundary conditions of the measurements with the mentioned optical system the surface data had to be filtered using a denoising wavelength of $\lambda_s = 2 \mu\text{m}$ and a cut-off-wavelength of at least $\lambda_c = 0.1 \text{ mm}$ [27]. In order to obtain more representative data, a larger quadratic measuring field with dimensions of $(0.5 \times 0.5) \text{ mm}^2$ was selected requiring an increased cut-off-wavelength with a value of $\lambda_c = 0.5 \text{ mm}$. Subsequently, the acquired primary surfaces were clipped to the defined quadratic measuring fields and levelled using subtraction method. Eventually, the filtered surface data were evaluated with regard to five-peaks

arithmetic mean height $S5p$, five-pits arithmetic mean height $S5v$, and valley void volume Vvv . Each of the sets of surface parameters was determined based on five measuring fields distributed over the generated surface of each specimen. Each of the investigated process parameter combinations was realised based on three separate specimens. Furthermore, a specific value was considered an outlier, if it exceeded an interval of $S5i = \overline{S5i} \pm 1.75 \cdot \sigma_{S5i}$ or $Vvv = \overline{Vvv} \pm 1.75 \cdot \sigma_{Vvv}$ with regard to the respective group of measurements.

The physical properties of the generated surfaces were characterised with regard to the resulting residual stress state. The residual stresses were determined based on $\sin^2 \psi$ -method with an instrument of the type Bruker Discover D8 (Bruker Corporation, Billerica, MA, USA) using an X-ray tube featuring a Co-anode. The diffraction planes angles of the lattice structure were measured with reference to the crystallographic planes $\{311\}$ presented according to Figure 4.

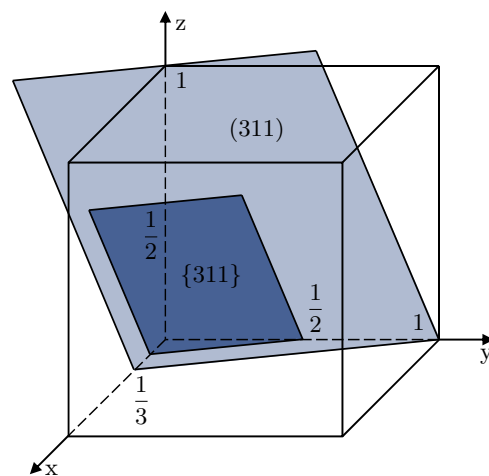


Figure 4. Orientation of the crystallographic planes $\{311\}$ considered for residual stress evaluation according to [24].

The measurements were realised in a measuring field with a diameter of 0.5 mm. The residual stress assessment was addressing the aluminium matrix, thus respecting the elastic parameters of the lattice with a Poisson's ratio $\nu_{\{311\}} = 0.35$ and a Young's modulus of $E_{\{311\}} = 69$ GPa. The presented results are based on measurements of two generated surfaces at separate specimens. The residual stress state of the SiC particles was not addressed.

3. Results and Discussion

The presented results are original data acquired by the evaluation of geometrical and physical properties of experimentally generated surfaces. The assigned milling experiments and evaluations were conducted as described in Section 2 (Materials and Methods).

3.1. Surface Structure

According to Figure 5 the addressed areal and volumetric surface parameters are presented in order to discuss the influence of the investigated tool geometries on the resulting structure of the generated surfaces. The given data represent averaged values and an error estimation is given based on the standard deviation.

On average, areal roughness values in the range below $0.2 \mu\text{m}$ were obtained for the investigated process parameters. The application of a chamfered corner combined with a straight cutting edge was addressed for different cutting edge angles. In this regard, the lowest cutting edge angle entailed the strongest fluctuations of the investigated areal surface parameters for all investigated geometries. Increased cutting edge angles typically led to reduced average values and fluctuations. One reason of these effects is seen within the increased tool contact length in the transition area between corner and minor

cutting edge with a decreased cutting edge angle. Similar results were obtained with the combination of a corner radius and a trailing cutting edge leading to strong fluctuations for the areal parameters as well. In this regard, the explanation based on an increased tool contact length is applicable as well, as the corner is followed by a section with a 0° tool cutting edge angle. As a result, the tendency to reoccurring tool deflection was increased, leading to stronger and to some extent random irregularities on the generated surfaces (Figure 6a,c). When applying the combination of a corner radius and a straight minor cutting edge the average values of the areal peak and valley parameters converged. This indicates a more regular structure of the machined surface as the height values of the peaks and valleys approximated (Figure 6b). The lowest roughness values were achieved using the combination of a corner radius and an arched minor cutting edge. With reference to that, the average values of the areal roughness parameters were in close proximity to each other representing a highly homogeneous surface (Figure 6d). The main reason for that is seen within the large effective radius generating the surface structure. In addition to a strongly reduced kinematic roughness the specific geometrical characteristics of the cross section of the uncut chip are assumed to benefit a stable cutting process.

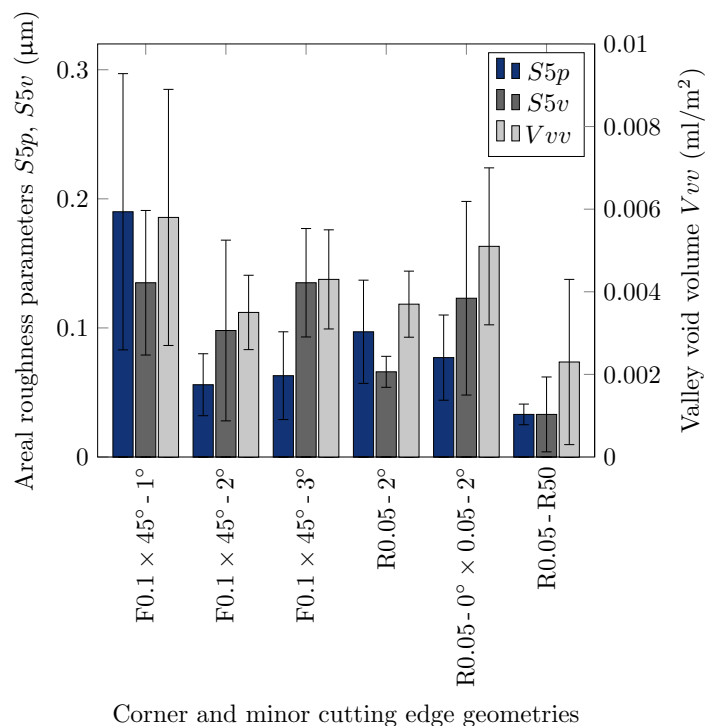


Figure 5. Areal and volumetric surface parameters of the generated surfaces depending on tool cutting edge angle, corner geometry, and minor cutting edge geometry ($v_c = 250 \text{ m/min}$, $f_z = 0.015 \text{ mm}$, $a_p = 0.25 \text{ mm}$, $a_e = 0.5 \text{ mm}$).

Schubert and Nestler achieved similar results when applying an arched wiper geometry in turning of a particle-reinforced AMC. In difference to the presented results, comparably low surface roughness values were also achieved with trailing cutting edges [18].

Generally, further scientific works such as Basheer et al., Nestler, and Sivasankaran et al. confirmed the effect of larger corner radii and thus the influence of increased effective radii on the surface structure [28], ([29], p. 117), Sivasankaran et al. [30].

With regard to the valley void volume, fluctuations were found for the smallest cutting edge angle and the trailing cutting edge as well. Additionally, the arched minor cutting also led to comparably strong fluctuations. Referring to the averaged values, the combination of a medium cutting edge angle with both of the investigated corner geometries enabled a decrease in the achievable valley void volumes. Despite the strong fluctuations, the arched

minor cutting edge on average led to the lowest values of the volumetric parameter in the investigated range.

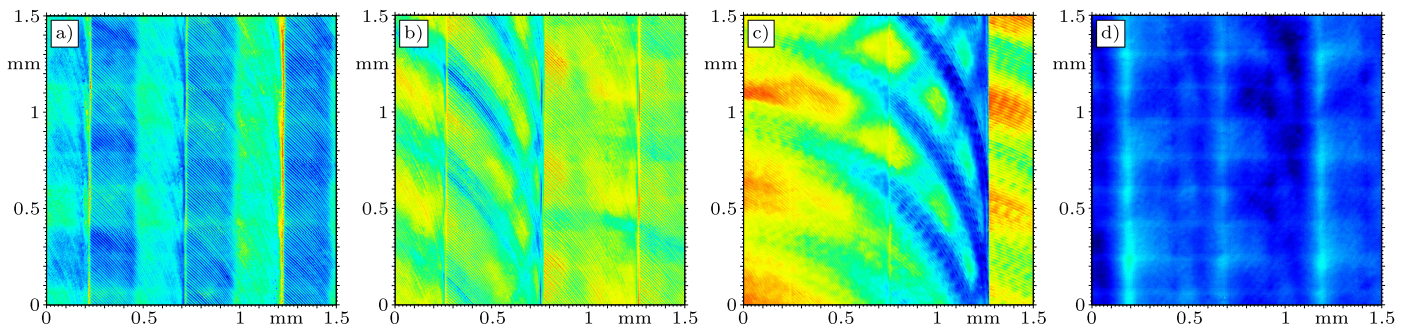


Figure 6. Surface structure of surfaces generated with (a) $F0.1 \times 45^\circ\text{-}1^\circ$, (b) $R0.05\text{-}2^\circ$, (c) $R0.05\text{-}0^\circ \times 0.05\text{-}2^\circ$, and (d) $R0.05\text{-}R50$ ($v_c = 250$ m/min, $f_z = 0.015$ mm, $a_p = 0.25$ mm, $a_e = 0.5$ mm).

Figure 6 presents selected generated surfaces in the form of pseudo colour images for an easier depiction of the surface features. In this regard, the surface representations are based on a unified range of height values to establish comparability. Furthermore, the different height values are indicated by contrasting colour values. For a better overview of the surface features the plots comprise a larger surface area of (1.5×1.5) mm². Moreover, the unfiltered primary surfaces were illustrated.

The strong fluctuations presented for certain tool geometries in Figure 5 are affirmed by strongly irregular surfaces and thus contrasting colour values in Figure 7a,c. The machined surfaces produced with the combination of a chamfered corner, a straight cutting edge and the smallest cutting edge angle featured distinct height differences between the surfaces inside each tool path compared to the ridges resulting in the transition zones between adjacent tool paths (Figure 7a). These surface regions are assigned to a feed motion angle $\phi = 180^\circ$ which represents the tool exit area. When using the tool geometry with a trailing cutting edge the strongest alternations of the surface structure were located in the same area. Moreover, the width of cut was distinguishable only in certain areas of the machined surface, while the larger proportion of the surface appeared to be generated in a single tool path with a larger width of cut. The main reason for that is seen within a higher tendency towards tool deflection caused by the increased tool contact length in the transition range between tool corner and minor cutting edge featuring a cutting edge angle of $\kappa'_r = 0^\circ \times 0.05$ (Figure 7c). A more homogeneous surface structure was obtained when applying the combination of a corner radius and a straight minor cutting edge, indicated by less distinct colour values of the pseudo colour image (Figure 7b). Eventually, the surface generated with an arched edge was characterised by the highest homogeneity in terms of the surface structure. Comparable colour values throughout the whole primary surface indicate a close proximity of the peaks and valleys without protruding ridges (Figure 7d).

3.2. Residual Stress State

Figure 7 presents the resulting residual stress state of surfaces generated with different cutting edge angles, corner geometries, and cutting edge geometries of the minor cutting edge.

Generally, the application of all investigated tool geometries resulted in the generation of higher absolute values of the compressive residual stresses compared to the initial state prior to milling. Typically finishing of AMCs is reported to result in compressive residual stress states such as in Wang et al. addressing milling of a particle-reinforced composite with PCD-tipped tools. In difference to that, machining of the unreinforced aluminium matrix entailed tensile residual stresses [15]. For the presented results, machining with increased cutting edge angles of the minor cutting edge on average led to a decreasing trend of the compressive residual stresses. Especially, the second principal stresses showed a steady decreasing trend in this regard. Furthermore, increasing fluctuations of the stress

values were determined with the increase in the cutting edge angle. Machining with a corner radius resulted in significantly stronger compressive residual stresses compared to the chamfered corner geometry and the strongest compressive residual stresses in the investigated range. Moreover, on average stronger compressive residual stresses were achieved with a combination of a corner radius and a straight minor cutting edge compared to a trailing minor cutting edge. With reference to that, considerable fluctuations of the residual stress state resulted when applying a trailing cutting edge. Eventually, the combination of a corner radius and a straight minor cutting edge generated significantly stronger compressive stresses compared to a corner radius combined with an arched minor cutting edge. In this context, the main geometrical difference is given by the effective tool radius generating the surface, which was substantially larger for the arched minor cutting edge. According to the findings, it can be deduced that small effective radii generating the surface entail strong compressive residual stresses. Lin et al. reported on similar results when turning a particle-reinforced AMC with CBN-tipped tools. The highest absolute compressive residual stresses were achieved with the smallest corner radius, while larger radii entailed an increased thickness of the affected surface layer [31]. Schubert, Nestler, and Mehner achieved the strongest compressive residual stresses in turning of a particle-reinforced AMC with a feed of 0.2 mm and CVD-D-tipped tools when applying the smallest corner radius. This was attributed primarily to changed effective tool cutting edge angles with different corner radii [32]. Additionally, Schubert et al. reported that strong compressive stresses within the cutting zone could be achieved applying a small corner radius [17]. The mechanical stresses during cutting may also effect the resulting residual stress state.

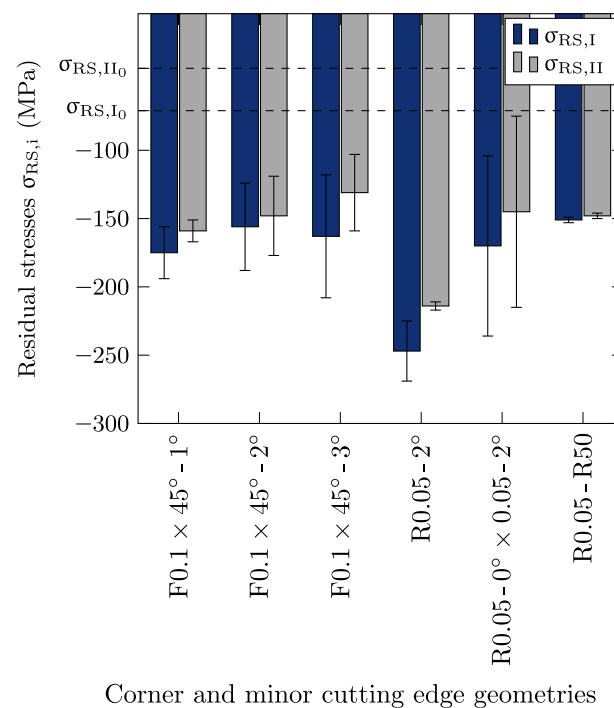


Figure 7. Residual stress state of the generated surfaces depending on tool cutting edge angle, corner geometry, and minor cutting edge geometry ($v_c = 250$ m/min, $f_z = 0.015$ mm, $a_p = 0.25$ mm, $a_e = 0.5$ mm).

4. Summary and Conclusions

The presented investigations addressed milling of a SiC particle-reinforced aluminium wrought alloy using MCD-tipped tools. Based on cutting experiments the influence of different corner and minor cutting edge geometries on the resulting geometrical and physical surface properties was focused. On average areal surface roughness values were achieved

in a range below 0.2 μm . In this regard, finishing with the smallest cutting edge angle of the minor cutting edge or a trailing minor cutting edge led to the strongest fluctuations of the surface parameter values. A medium cutting edge angle of the minor cutting edge combined with both of the investigated corner geometries allowed for decreased valley void volumes. On average, the lowest values of the volumetric surface parameter were achieved with the tool featuring an arched minor cutting edge. Moreover, finishing with any of the investigated tool geometries led to an increase in the compressive residual stresses compared to the state prior to machining. The highest average absolute values of compressive residual stresses were achieved with the combination of a small corner radius and a straight minor cutting edge. The results support the assumption, that the surface generation by small effective radii enables stronger compressive residual stresses in difference to larger effective radii when machining with an arched edge. Accordingly, further investigations should address different corner radii in a more detailed manner.

Author Contributions: Conceptualisation, B.C. and A.S.; Data curation, B.C.; Formal analysis, B.C.; Investigation, B.C.; Project administration, A.S.; Resources, A.S.; Visualisation, B.C.; Writing—original draft, B.C.; Writing—review and editing, B.C. and A.S. All authors have read and agreed to the published version of the manuscript.

Funding: This research was funded by Deutsche Forschungsgemeinschaft (DFG, German Research Foundation) grant number 14208545 in the framework of the Collaborative Research Centre SFB 692 HALS at Chemnitz University of Technology.

Institutional Review Board Statement: Not applicable.

Informed Consent Statement: Not applicable.

Data Availability Statement: The data presented in this study are available on request from the corresponding author. The data are not publicly available due to ongoing research activities.

Acknowledgements: The publication of this article was funded by Chemnitz University of Technology.

Conflicts of Interest: The authors declare no conflict of interest. The funders had no role in the design of the study; in the collection, analyses, or interpretation of data; in the writing of the manuscript, or in the decision to publish the results.

Abbreviations

The following abbreviations and symbols are used in this manuscript:

a_e	Width of cut
a_p	Depth of cut
A_g	Fracture elongation
AMC	Aluminium matrix composite
CBN	Cubic boron nitride
CVD	Chemical vapour deposition
CVD-D	Chemical vapour deposited diamond
d_{90}	Average particle diameter for 90% particle proportion
E	Young's modulus
$E_{\{311\}}$	Young's modulus for X-ray diffraction analysis
ECM	Electro chemical machining
f_z	Feed per tooth
HSS	High speed steel
HV 10	Vickers hardness
MCD	Mono crystalline diamond
MMC	Metal matrix composite
n_{Sp}	Rotational speed of milling spindle
ND	Natural diamond
PCD	Poly crystalline diamond
R_m	Ultimate tensile strength

$R_{p0.2}$	Yield strength
$\overline{S5p}$	Five-peaks arithmetic mean height
$\overline{S5p}$	Average five-peaks arithmetic mean height
$\overline{S5v}$	Five-pits arithmetic mean height
$\overline{S5v}$	Average five-pits arithmetic mean height
SEM	Scanning electron microscopy
v_c	Cutting speed
V_{vv}	Valley void volume
α'_o	Clearance angle of the minor cutting edge
β'_o	Wedge angle of the minor cutting edge
γ'_o	Rake angle of minor cutting edge
κ'_r	Tool cutting edge angle of the minor cutting edge
λ_c	Cut-off wavelength
λ_s	Denoising wavelength
$\nu_{\{311\}}$	Poisson's ratio for X-ray diffraction analysis
σ_{S5i}	Standard deviation of five-peaks or five-pits parameters
$\sigma_{V_{vv}}$	Standard deviation of valley void volume
$\sigma_{RS,I}$	First principal residual stress
σ_{RS,I_0}	Initial first principal residual stress
$\sigma_{RS,II}$	Second principal residual stress
σ_{RS,II_0}	Initial second principal residual stress
ϕ	Feed motion angle

References

- Batraev, I.; Chaitanya, S.; Cheng, X.; Dudina, D.V.; Krishnaraj, V.; Kumar, R.; Li, Y.; Lu, W.; Manna, A.; Jordá, J.M.; et al. *Metal Matrix Composites: Materials, Manufacturing and Engineering*, 1st ed.; De Gruyter: Berlin, Germany, 2014.
- Akhil, R. A Study on Recent Trends in the Applications of Metal Matrix Composites. *Int. J. Res. Appl. Sci. Eng. Technol.* **2018**, *6*, 172–180.
- Schmidt, A.; Siebeck, S.; Götze, U.; Wagner, G.; Nestler, D. Particle-Reinforced Aluminum Matrix Composites (AMCs)—Selected Results of an Integrated Technology, User, and Market Analysis and Forecast. *Metals* **2018**, *8*, 143. [[CrossRef](#)]
- Shishkin, A.; Mironov, V.; Goljandin, D.; Lapkovsky, V. Recycling of Al-W-B composite material. *Key Eng. Mater.* **2012**, *527*, 143–147. [[CrossRef](#)]
- Guo, Z.; Li, Q.; Shu, G. Evolution of microstructure and mechanical properties of the Al-B₄C composite after recycling. *IOP Conf. Ser. Mater. Sci. Eng.* **2018**, *409*, 1–8. [[CrossRef](#)]
- Hung, N.P.; Boey, F.Y.; Khor, K.A.; Oh, C.A.; Lee, H.F. Machinability of cast and powder-formed aluminum alloys reinforced with SiC particles. *J. Mater. Process. Technol.* **1995**, *48*, 291–297. [[CrossRef](#)]
- Yanming, Q.; Zehua, Z. Tool wear and its mechanism for cutting SiC particle-reinforced aluminium matrix composites. *J. Mater. Process. Technol.* **2000**, *100*, 194–199. [[CrossRef](#)]
- Ding, X.; Liew, W.Y.H.; Liu, X.D. Evaluation of machining performance of MMC with PCBN and PCD tools. *Wear* **2005**, *259*, 1225–1234. [[CrossRef](#)]
- Bushlya, V.; Lenrick, F.; Gutnichenko, O.; Petrusha, I.; Osipov, O.; Kristiansson, S.; Stahl, J.E. Performance and wear mechanisms of novel superhard diamond and boron nitride based tools in machining Al-SiCp metal matrix composite. *Wear* **2017**, *376–377*, 152–164. [[CrossRef](#)]
- Wang, T.; Xie, L.; Wang, X.; Ding, Z. PCD tool performance in high-speed milling of high volume fraction SiCp/Al composites. *Int. J. Adv. Manuf. Technol.* **2015**, *78*, 1445–1453. [[CrossRef](#)]
- Collins, J.L.; Cook, M.W. Machining MMCs with Diamond Tools. In Proceedings of the Tribology 2000—Plus, 12th International Colloquium, Ostfildern, Germany, 11–13 January 2000; Volume 3, pp. 1837–1853.
- Cooper, J.O. Machining of metal matrix composites using PCD, natural diamond, single crystal CVD and polycrystalline CVD diamond. *Ind. Diam. Rev.* **2007**, *67*, 34–38.
- Bushan, R.K.; Kumar, S.; Das, S. Effect of machining parameters on surface roughness and tool wear of 7075 Al alloy SiC composite. *Int. J. Adv. Manuf. Technol.* **2010**, *50*, 459–469. [[CrossRef](#)]
- Ge, Y.; Xu, J.; Fu, Y. Experimental study on high-speed milling of SiCp/Al composites. *Adv. Mater. Res.* **2011**, *291–294*, 725–731. [[CrossRef](#)]
- Wang, T.; Xie, L.J.; Wang, X.B.; Jiao, L.; Shen, J.W.; Xu, H.; Nie, F.M. Surface Integrity of High Speed Milling of Al/SiC/65p Aluminum Matrix Composites. *Procedia CIRP* **2013**, *8*, 475–480. [[CrossRef](#)]
- Dong, G.J.; Zhang, Y.J.; Zhou, M.; Wang, Y.J. The research of effect of cutting parameters on machined surface defects in high-speed milling of SiCp/Al composites. *Key Eng. Mater.* **2013**, *589–590*, 245–251. [[CrossRef](#)]

17. Schubert, A.; Nestler, A.; Schmidt, T.; Schneider, J. Finishing of Aluminium Based Light Weight Materials. Sustainable production for resource efficiency and ecomobility. In Proceedings of the International Chemnitz Manufacturing Colloquium, Chemnitz, Germany, 29–30 September 2010; Neugebauer, R., Ed.; pp. 447–464.
18. Schubert, A.; Nestler, A. Enhancement of surface integrity in turning of particle reinforced aluminium matrix composites by tool design. *Procedia Eng.* **2011**, *19*, 300–305. [[CrossRef](#)]
19. Clauß, B.; Nestler, A.; Schubert, A. Investigation of Surface Properties in Milling of SiC Particle Reinforced Aluminium Matrix Composites (AMCs). *Procedia CIRP* **2016**, *46*, 480–483. [[CrossRef](#)]
20. Ge, Y.F.; Xu, J.H.; Yang, H.; Luo, S.B.; Fu, Y.C. Workpiece surface quality when ultra-precision turning of SiCp/Al composites. *J. Mater. Process. Technol.* **2008**, *203*, 166–175. [[CrossRef](#)]
21. Bian, R.; He, N.; Li, L.; Zhan, Z.B.; Wu, Q.; Shi, Z.Y. Precision milling of high volume fraction SiC_p/Al composites with monocrystalline diamond end mill. *Int. J. Adv. Manuf. Technol.* **2013**, *71*, 411–419. [[CrossRef](#)]
22. Clauß, B.; Nestler, A.; Schubert, A.; Dietrich, D.; Lampke, T. Investigation of surface properties in turn milling of particle-reinforced aluminium matrix composites using MCD-tipped tools. *Int. J. Adv. Manuf. Technol.* **2019**, *105*, 937–950. [[CrossRef](#)]
23. Clauß, B.; Nestler, A.; Schubert, A.; Dietrich, D.; Lampke, T. Influencing the Properties of the Generated Surface by Adjusted Rake and Clearance Angles in Side Milling of Aluminium Matrix Composites with MCD-Tipped Tools. *J. Manuf. Mater. Process.* **2019**, *3*, 59.
24. Clauß, B.; Nestler, A.; Mehner, T.; Schubert, A.; Lampke, T. Influence of SiC particle volume fraction and texture on the surface properties in milling of AMCs with MCD-tipped tools. *Procedia CIRP* **2019**, *85*, 90–95. [[CrossRef](#)]
25. Siebeck, S. Powder Metallurgical Synthesis of Aluminum Matrix Composites by Means Ofhigh Energy Milling. Ph.D. Thesis, Chemnitz University of Technology, Chemnitz, Germany, 2018.
26. Hockauf, M.; Wagner, M.F.; Händel, M.; Lampke, T.; Siebeck, S.; Wielage, B. High-strenght aluminium-based light-weight materials for safety components—Recent progress by microstructural refinement and particle reinforcement. *Int. J. Mater. Res.* **2012**, *103*, 3–11. [[CrossRef](#)]
27. DIN EN ISO 25178-3. *Geometrical Product Specifications (GPS)—Surface Texture: Areal—Part 3: Specification Operators (ISO 25178-3:2012)*; Deutsches Institut für Normung e. V.: Berlin, Germany, 2012.
28. Basheer, A.C.; Dabade, U.A.; Joshi, S.S.; Bhanuprasad, V.V.; Gadre, V.M. Modeling of surface roughness in precision machining of metal matrix composites using ANN. *J. Mater. Process. Technol.* **2008**, *197*, 439–444. [[CrossRef](#)]
29. Nestler, A. Erzeugung Definierter Oberflächeneigenschaften bei der Drehbearbeitung von Partikelverstärkten Aluminiummatrix-Verbundwerkstoffen. Ph.D. Thesis, Chemnitz University of Technology, Chemnitz, Germany, 2013.
30. Sivasankaran, S.; Harisagar, P.T.; Saminathan, E.; Siddharth, S.; Sasikumar, P. Effect of nose radius and graphite addition on turning of AA 7075-ZrB₂ in-situ composites. *Procedia Eng.* **2014**, *97*, 582–589. [[CrossRef](#)]
31. Lin, K.; Wang, W.; Jiang, R.; Xiong, Y. Effect of tool nose radius and tool wear on residual stresses distribution white turning in situ TiB₂/7050 Al metal matrix composites. *Int. J. Adv. Manuf. Technol.* **2019**, *100*, 143–151. [[CrossRef](#)]
32. Schubert, A.; Nestler, A.; Mehner, T. Influencing the residual stresses in the surface layer by use of appropriate cutting parameters and tool geometries in turning of aluminium matrix composites. *Mater. Werkst.* **2012**, *43*, 648–655. [[CrossRef](#)]